UNIVERSITY OF MICHIGAN — Michigan Engineering

NERS/BIOE 481

Lecture 10
X-ray Imaging Detectors

Michael Flynn, Adjunct Prof
Nuclear Engr & Rad. Science
mikef@umich.edu
mikef@rad.hfh.edu

Henry Ford Health System
RADIOLOGY RESEARCH

General Models

Radiographic Imaging: Subject contrast (A) recorded by the detector (B) is transformed (C) to display values presented (D) for the human visual system (E) and interpretation.

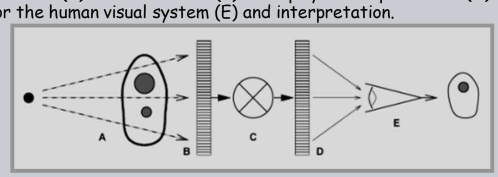

Radioisotope Imaging: The detector records the radioactivity distribution by using a multi-hole collimator.

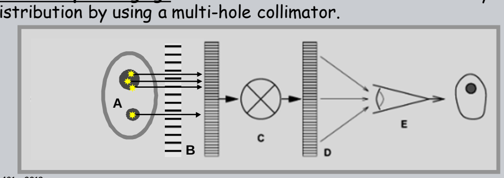

Intro Acquisition methods

- Early Digital Radiography methods.
  1. Photostimulable phosphor (PSP) imaging (often called Computed Radiography or CR)
     Agfa Carestream
     Fuji Konica
  2. CCD camera with Gd_2O_2S / CsI
     SwissRay Oldelft
     Imaging Dynamics DIRA
- Current Digital Radiography Technologies.
  3. Amorphous selenium with TFT arrays
     Hologic Shimadzu
     Siemens Fuji
  4. Photodiode arrays coupled with CsI
     GE Canon Carestream
     Trixell (Siemens, Philips, Thompson)

VI.C.1 – Computed Radiography, CR (13 charts)

1) Computed Radiography, CR
   a) Photostimulable (storage) Phosphors
   b) CR Reader
   c) Advanced designs
   d) Performance – MTF/DQE
   e) artifacts

CR history

Storage Phosphor Radiography
(computed radiography)

- The most common digital radiographic modality
- Invented by G.W. Luckey at Eastman Kodak Co. in 1975
- First commercial unit introduced in 1983 (Fuji FCR 101)

- Exposed cassettes are processed in a remote reader using the same operational paradigm as for processed film.
- Common in medicine & industry.
- Easily replaces film-screen cassettes and film processors.

---

a - CR Latent Image

- Formation of the latent image
  - Excitation of e^- to the conduction band upon x-ray exposure
  - Deposition of the e^-'s in the energy traps within the conduction band created by the impurities in the phosphor structure

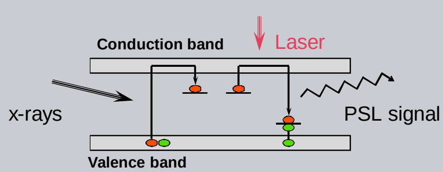

- Reading the latent image
  - stimulation (detrapping) of the trapped e^-s with a laser beam and collecting the photo-stimulated luminescent (PSL) signal

a - CR Photostimulable luminescence

Photostimulable luminescence (PSL)

- Emission of light (PSL signal) from a material (phosphor screen) in an excited state (exposed) upon stimulation by visible light (scanning laser beam)
- Phosphor BaFX:Eu (X = Br or I)

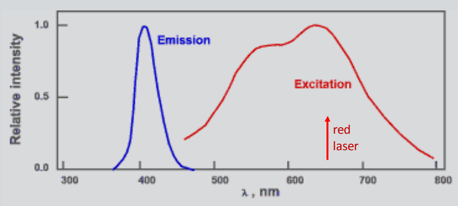

b - CR scanned laser readout

Laser scanned plate readout

- A rotating polygon mirror scans a laser spot across a phosphor plate.
- The stimulated release of light is recorded and the position is registered.

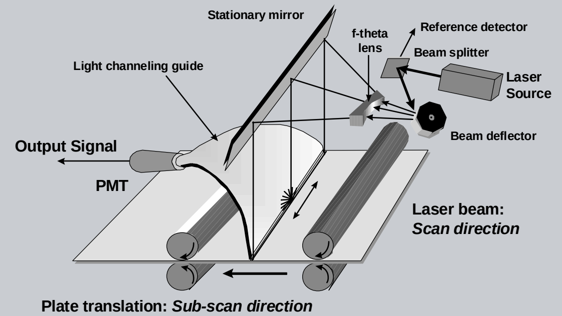

b - CR specifications.

- Typical Signal:
  - ~.01 mR minimum to ~10 mR maximum (10^4 range)
  - 10 bit (1024) or 12 bit(4096) log signal recorded.
- Typical Sizes:

Size / Type (inches)	Digital Matrix	Pixel Size (mm)	Nyquist Frequency (cylcles/mm)	File Size (Mbytes)
14 x 17 / ST	1760 x 2140	0.2	2.5	7.533
10 x 12 / ST	1760 x 2010	0.15	3.33	7.075
8 x 10 / ST	2000 x 2510	0.1	5	10.04
8 x 10 / HR	2000 x 2510	0.1	5	10.04

c - CR new methods: scanhead readout (1D)

From Seibert, 2007

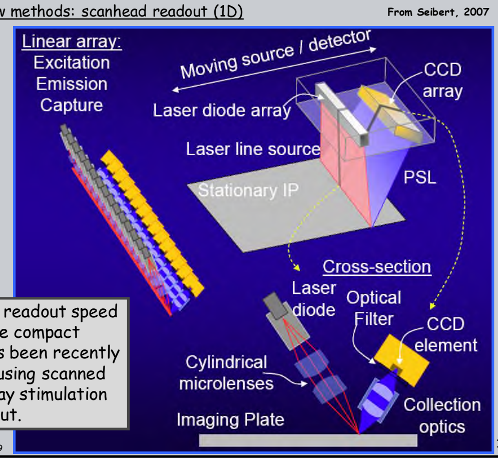

Improved readout speed and a more compact design has been recently achieved using scanned linear array stimulation and readout.

c - CR new methods: needle phosphor material

Introduced recently by Agfa, CsBr:Eu^{2+} needle shaped storage phosphor crystals permit thicker phosphor screens for same light blur in comparison with traditional granular phosphor screens.

Illustration from:

- US Patent 6967339
- 22-NOV-2005
- Agfa-Gevaert, Mortsel (BE)

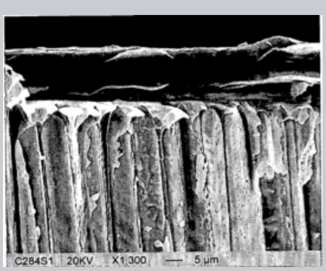

c - CR: needle vs granular phosphor

Needle screen is thicker with better x-ray absorption and lower noise.

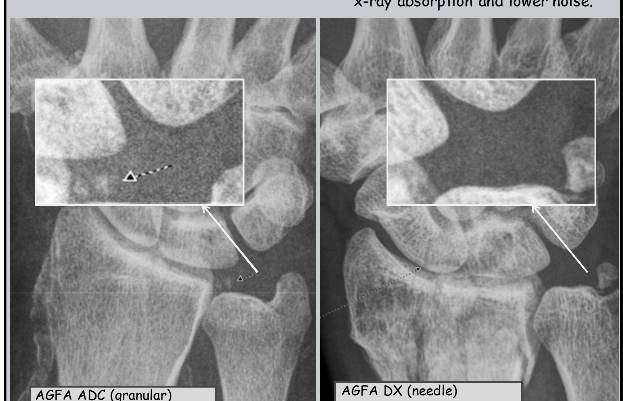

d. Image Blur from Light Diffusion

1. X-rays are absorbed in storage phosphors (light blue).
2. A focused laser beam (red) scatters within the screen before stimulating light release.
3. Released light (blue) further scatters before leaving the surface of the screen.
4. Emitted light is detected by a large area photo-detectors (PD)

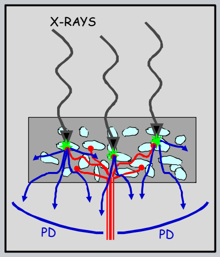

- Blur in computed radiography results from laser light lateral diffusion prior to stimulating light emission.
- For the same screen thickness, needle phosphor screens have less blur than granular phosphors. However, needle phosphors screens are often thicker for improved absorption.
- No further blur results from diffusion of the emitted light.

d - CR Physical Performance

KCARE Report #06004
Agfa Healthcare DX-S
March 2006

Modulation Transfer Function (MTF)

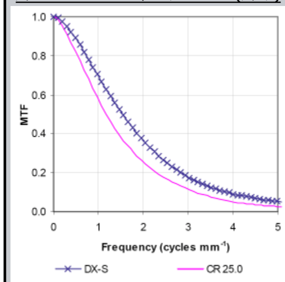

Detective Quantum Efficiency (DQE)

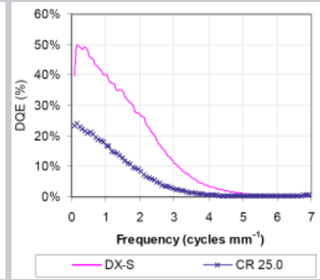

DX-S - Agfa scanhead/needle phosphor system
CR 25.0 - Agfa conventional computed radiography system.

e - CR artifacts

CR specific artifacts

- Incorrect image processing
- Segmentation error (mispositioning)
- → White specks (unclean screens)
- White traces (cracked screens)
- Vertical bands (dirty light guide)
- Multiple images (non-erased screens)
- → Moiré pattern (due to the grid)
- Aliasing
- Print artifacts

e - CR Dust artifact

Dust on a CR screen blocks laser readout. Periodic screen cleaning is required.

e - CR Grid artifact

A moire artifact resulting from the laser scan direction being nearly parallel to a grid with too large a spacing.

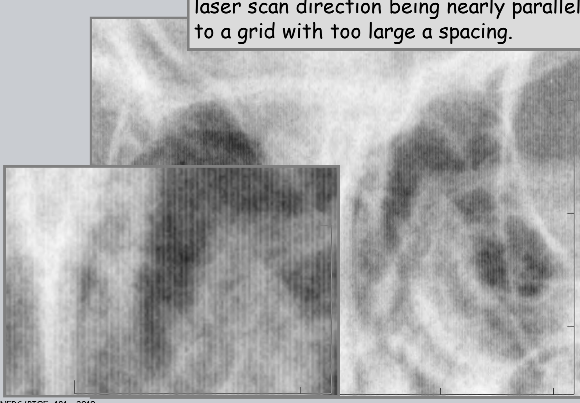

VI.C.2 - CCD systems, (8 charts)

2) Phosphor - CCD systems
 a) Lens coupled design
 b) Light collection efficiency.
 c) Methods for improved light collection
 d) Charge Coupled Devices, CCD
 e) Folded optics
 f) Gantry mount
 g) Focus problems
 h) Small FOV designs (fiber coupled)

a - Lens coupled CCD camera

Light from a scintillation phosphor screen is recorded using a lens and a focal plane CCD sensor

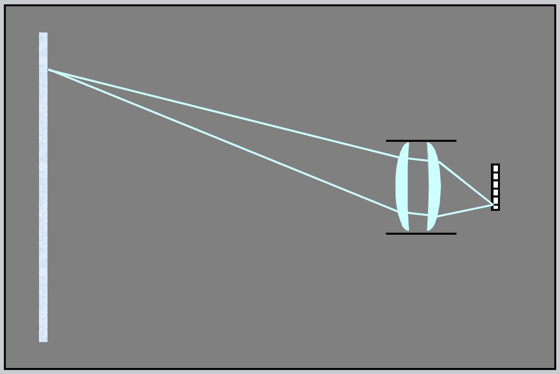

b - Lens coupled CCD camera

Lens couples system suffer from poor light collection efficiency

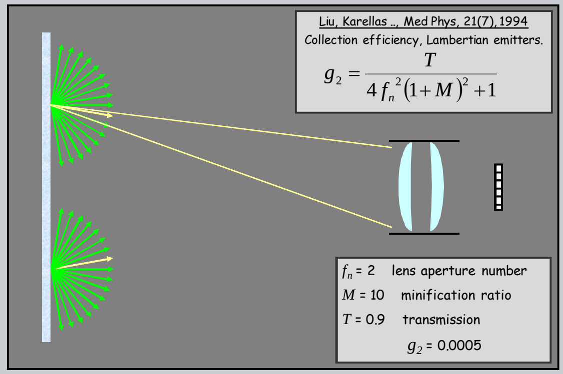

b - Excess noise from poor light collection

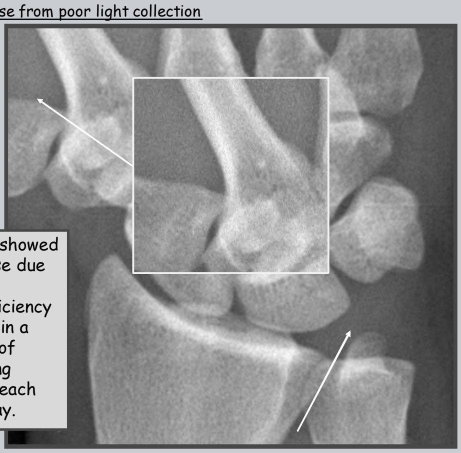

Early designs showed excessive noise due to poor light collection efficiency that resulted in a small number of electrons being produced for each absorbed x-ray.

c - Lens coupled CCD camera

Four methods have been used to improve the light collection efficiency

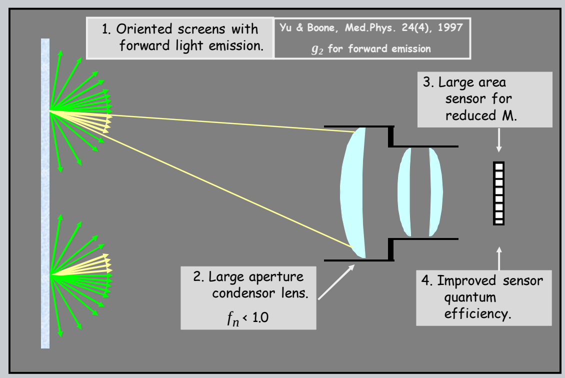

d - Large area, high QE CCD sensors

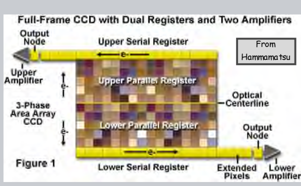

Large area, full frame transfer sensors are made by Eastman Kodak Co. with a thin film surface that promotes short wavelength absorption

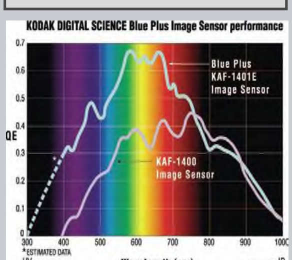

39 mm x 50 mm Kodak 22 MP sensor

e - Lens coupled CCD camera

More compact designs are achieved by using a mirror (folded optics)

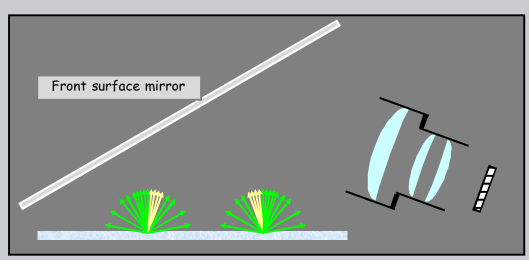

g - Gantry Mounted CCD detector

Imaging Dynamic Company Ltd (IDC)
Calgary, AB, Canada
www.imagingdynamics.com

g -Blur artifacts

While current designs do not suffer from added noise, the systems are susceptible to blur artifacts due to the lens coupling being out of focus.

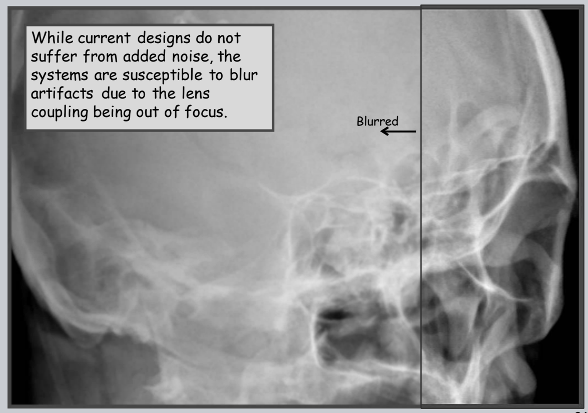

VI.C.3 – Flat panel Digital Radiography, DR (20 charts)

3) Digital Radiography, DR
   a) DR detector panels
   b) DR systems integration
   c) Signal preprocessing
   d) Direct vs Indirect
   e) Artifacts

a. Detectors: DR

Amorphous Silicon Flat Panel Detectors

Flat panel digital radiography detectors integrate the absorption of radiation and the electronic readout in a single panel

Electronic circuits made of amorphous silicon form thin film transisters (AM-TFT) that read charge created by x-rays. The AM-TFT technology is similar to that used in common LCD displays

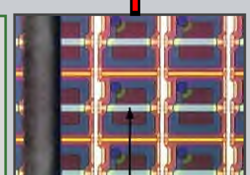

Human hair for size reference

a. Detectors: Direct & Indirect

Indirect: Each absorbed x-ray produces a burst of light in a phosphor screen. These light photons are absorbed by the photodetector and converted to electrical charge.

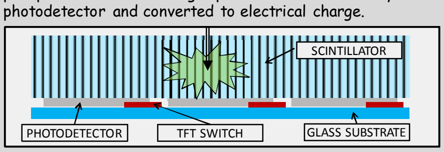

Direct: Each absorbed x-ray produces charge directly in a conductive material. This burst of charge is rapidly collected and stored on a capacitor.

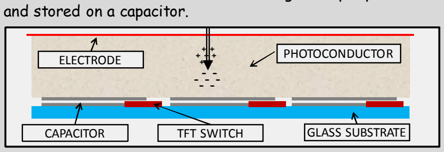

a. Detectors: TFT panel readout

- The charge collected at each pixel in a row is measured and converted to a digital number.
- All rows are sequentially addressed until the entire image is read and digitized.

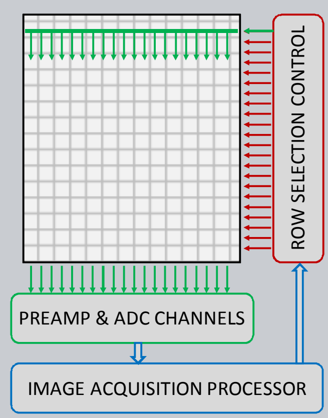

a. Detectors: DR pixels

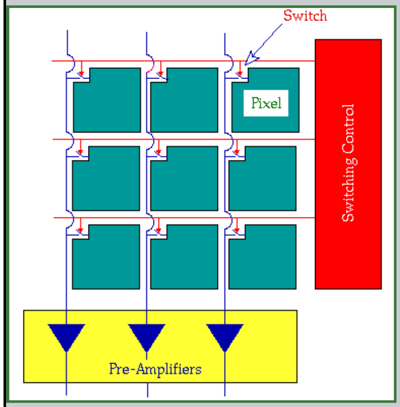

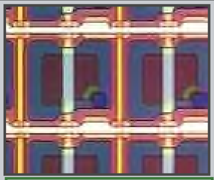

- The row address control circuits are used to connect all capacitors in a row to the readout lines.
- While the row is active, preamplifiers convert the charge on each pixel to a voltage for conversion using an analogue to digital convertor (ADC)

a. Detectors: Pixel details

At each pixel, amorphous silicon thin film circuits form a capacitor to store the signal charge and a switching transistor to activate readout

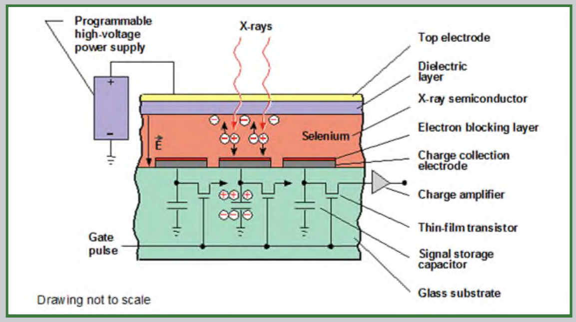

b. DR Integrated xray generators

Integration of the x-ray generator control with the detector allows technical parameters to be programmed for an exam.

→PACS Worklist
→Order Code
→ **Technique**
kVp
mA
S (timed)
grid
→ **Views**
AP
Lat
Townes

The image quickly appears on the radiographers screen so that the image quality, processing, and subject position can be confirmed.

c - DR 'For Processing' Data

RAW data from the detector is pre-processed to produce an image suitable for processing.

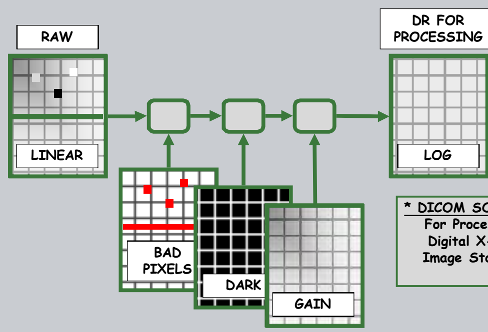

* DICOM SOP Class
For Processing
Digital X-ray
Image Storage

* DICOM UID 1.2.840.10008.5.1.4.1.1.1.1

c - Bad pixels

- Pixels with high or low values or with excessive noise
- Values corrected by interpolation from neighbors
- There are presently no requirements to report bad pixel statistics as a part of DR system purchase.

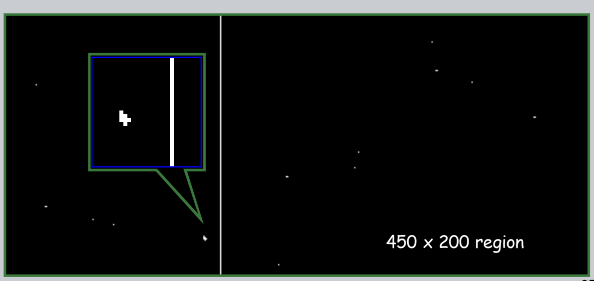

c - Dark image

- The signal recorded when no x-rays are incident on the detector is referred to as the 'dark image' or 'offset image'.
- Most detectors produce a signal that linearly increase from the offset value of each pixel as x-ray incident exposure is increased.
- Dark image values are susceptible to drift and often have high thermal dependence.

Digital Fluoroscopy dark image

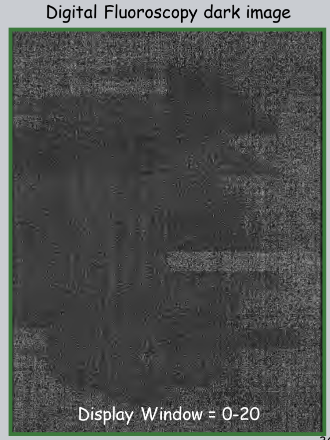

c - Offset/Gain correction

- Dark Image - I_D

  Obtained by averaging many images obtained with no xray input to the detector.

- Gain Image - I_G

  Obtained by averaging many images obtained with a uniform x-ray fluence.

- Uniformity correction is performed subtracting the dark offset and adjusting for gain differences.

$$I_{COR} = (I_{RAW} - I_D) \{k / (I_G - I_D)\}$$

- Log transformation using a Log look-up table allows this to be performed with a subtraction.

$$I_{FP} = log\,(I_{RAW} - I_D) - log(I_G - I_D) - K$$

c – log image values

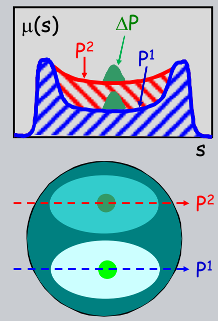

The linear signal is approximately proportional to the incident x-ray intensity;

$$I(x,y) \;\alpha\; I_o \; exp\{- P(x,y)\}$$

$$P(x,y) = \int_s \mu(s)ds$$

The log signal is proportional to the line integral.

$$Ln(I(x,y)) \;\alpha\; -P(x,y) + Ln(Io)$$

Small perturbations cause the same image value change whether in high or low transmission regions

$$I^1_{FP} \;\alpha\; P^1(x,y) + \Delta P$$

$$I^2_{FP} \;\alpha\; P^2(x,y) + \Delta P$$

c - DR 'For Presentation' Data

http://dicom.nema.org/

Image processing is applied to improve the visual presentation of low contrast details.

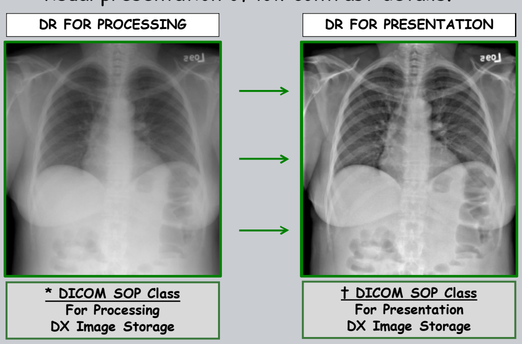

* DICOM UID 1.2.840.10008.5.1.4.1.1.1.1.1 † DICOM UID 1.2.840.10008.5.1.4.1.1.1.1

Note: L12 will describe image processing

d. Direct vs Indirect DR

- Indirect DR: lateral light transport in scintillator screens causes blur. For the same screen thickness, this is less for oriented fiber screens compared to granular screens. However, oriented fiber screen are typically thicker to achieve improved absorption with similar blur

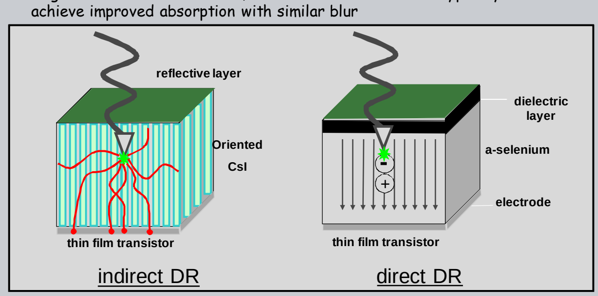

- Direct DR: Experiments with x-ray micro beams from a synchrotron have established that there is negligible blue in a direct DR detector. Charge is transported with minimal lateral movement.

d. DR MTF

KCARE report number 05078, October 2005.
Digital Detectors for General Radiography

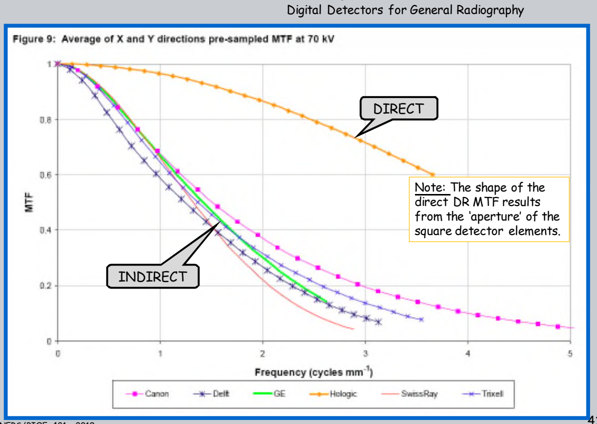

d. DR DQE

KCARE report number 05078, October 2005.
Digital Detectors for General Radiography

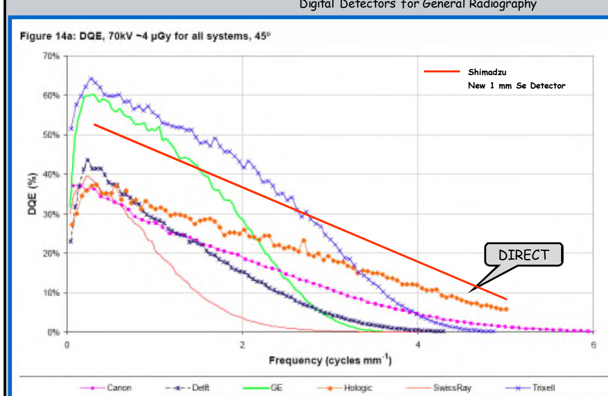

d. DR MTF

Hunter, Med. Phys., 2012

Measured and calculated K-fluorescence effects on the MTF of an amorphous-selenium based CCD x-ray detector

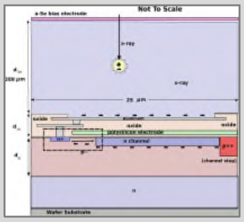

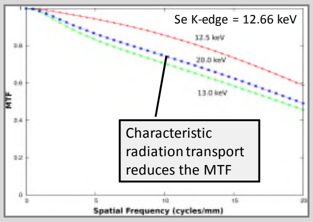

High resolution Se DR systems (25 micron pixels) are limited by radiation transport effects

Scott, SPIE MI, 2014
Amorphous selenium direct detection CMOS digital x-ray imager with 25 micron pixel pitch

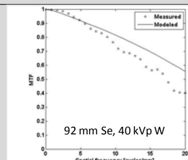

DR vs CR

DR systems offer several advantages relative to CR:

- Improved image quality (i.e MTF, NPS, DQE)
- Integrated system provides better productivity.

This has led to a decrease in the utilization of CR.

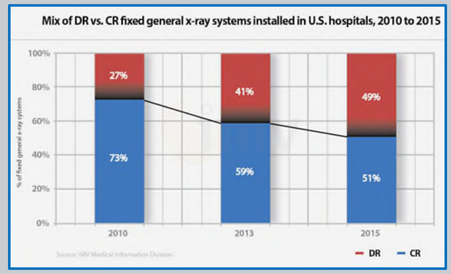

NOTE: The US Medicare system will began reducing payments for exams performed on CR systems beginning in 2018.

e. Detectors: DR artifacts

DR specific artifacts

- Pixel defects:
  - Circuit defects can make a single pixel or an entire column/row unresponsive to x-rays.
  - These defects are generally corrected by interpolation.
  - Excessive correction can mask small image details.
- Pixel gain variation:
  - For the same x-ray exposure, each pixel may produce a slightly different digital signal:
    - Area variations
    - Amplifier gain variations
  - A uniformity correction is done to prevent fixed pattern noise in the image.
  - Improper correction adds noise in addition to the normally present quantum mottle.

c – New Bad pixels

- New pixel defects can develop in DR panels that are in service.
- Frequent gain calibration can help detect newly developed problems.
- The defects shown to the right were reported by the radiologist interpreting the study.

c – Gain image

- The linear gain may slightly differ from pixel to pixel.
- These variations produce fixed pattern noise.

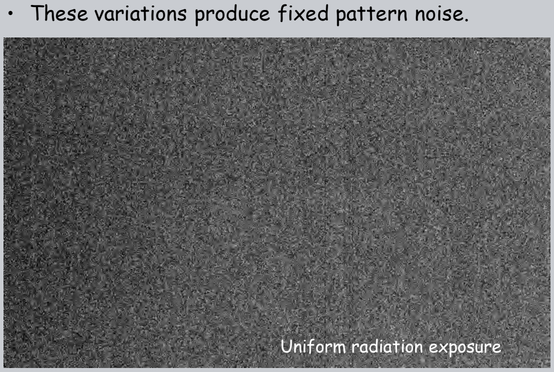

VI.C.4 – Radiographic Detective Efficiency - Theory (10 charts)

4) Large area detective effiency, DQE(0)

a. energy deposition distribution
b. signal
c. noise
d. DQE(0)
e. Signal difference and relative contrast

a - P(e,E)dE for a Selenium Photoconductor on glass

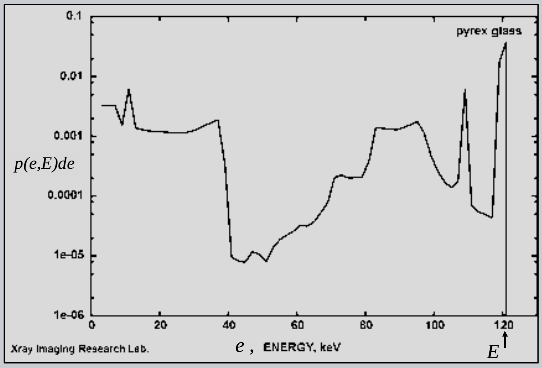

a - P(e,E)dE for a Selenium Photoconductor on glass

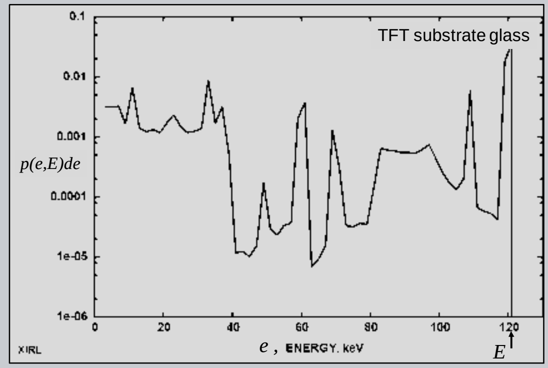

IV.C.3 – Ideal image detector – energy integrating type

From Lecture 05

- An ideal energy integrating detector will record a signal equal to the total energy of all photons incident on the detector surface.
- The detected signal for an ideal energy integrating detector, *Se*, can be written as:

$$S_e = A_d t \int_0^{E_{max}} E\phi(E)\, dE$$

Where

- t is the exposure time, sec
- ϕ is the photon fluence rate, photons/mm2/sec,
- A_d is the effective area of a detector element.

The majority of actual radiographic detectors are energy integrating; however, they are not 'ideal'.

b - Signal - actual detector, energy integrating - MONO-ENERGETIC.

- As a first step in deriving an expression for an actual detector, we write first the expression for monoenergetic x-rays.

$$S_E = \Phi_E \int_0^E ep(e,E)\,de$$

Note1: S_E and Φ_E are used to denote monoenergetic at E

- This can be used to define a signal detection efficiency.

$$\longrightarrow \quad \eta_s(E) = \frac{S_E}{E\Phi_E} = \int_0^E ep(e,E)\,de \Big/ E$$

Note2: For simplicity, we now write: $\Phi_E = A_d t \phi_E$

Note3: In a Monte Carlo analysis, the signal is determined by summing the energy deposited for H incident x-rays. The efficiency is trivially determined from this.

$$S_E = \sum_{i=1}^{H} e_i \qquad \eta_{S_E} = \frac{S_E}{EH}$$

c - Noise - actual detector, energy integrating - MONO-ENERGETIC.

- The noise can be similarly written as a second moment integral.

$$\sigma_E^2 = \Phi_E \int_0^E e^2 p(e,E)\,de$$

- And the noise transfer efficiency similarly defined.

$$\longrightarrow \quad \eta_\sigma^2(E) = \frac{\sigma_E^2}{E^2\Phi_E} = \int_0^E e^2 p(e,E)\,de \Big/ E^2$$

Note that this efficiency is the variance transfer.

Note: In a Monte Carlo analysis, the noise transfer and related efficiency is determined by accumulating the square of the energy deposited by each x-ray.

$$\sigma_E^2 = \sum_{i=1}^{H} e_E^2 \qquad \eta_{\sigma_E}^2 = \frac{\sigma_E^2}{E^2 H}$$

d - Signal and noise for a SPECTRUM of Xray Energies.

- For detectors with **linear signals**, the **signal and noise** are determined by **separate integrals** incorporating the efficiency.

$$\longrightarrow \quad S = \int_0^{kV} \eta_S(E) E \Phi(E)\,dE$$

Note1: $\Phi(E)$ is now used to denote the energy spectrum.

$$\longrightarrow \quad \sigma_S^2 = \int_0^{kV} \eta_\sigma^2(E) E^2 \Phi(E)\,dE$$

- For **multiple channels** which **linearly accumulate** signal, the energy absorption and noise power **efficiencies are additive**.

$$\eta_s(E) = \eta_{s_1}(E) + \eta_{s_2}(E) + \ldots \eta_{sn}(E)$$

$$\eta_\sigma^2(E) = \eta_{\sigma_1}^2(E) + \eta_{\sigma_2}^2(E) + \ldots \eta_{\sigma_n}^2(E)$$

d - SNR and DQE - MONO-ENERGETIC

Signal and Noise for a monoenergetic xray beam	NEQ (i.e. SNR²) and DQE for a monoenergetic x-ray beam
$S_E = \eta_s(E) E \Phi_E$	$\frac{S_E^2}{\sigma_{S_E}^2} = \frac{\eta_S^2(E)}{\eta_\sigma^2(E)} \Phi_E = NEQ$
$\sigma_{S_E}^2 = \eta_\sigma^2(E) E^2 \Phi_E$	$DQE_E = \frac{\eta_S^2(E)}{\eta_\sigma^2(E)}$

DQE_E was first reported by Swank in term of the moments, M_n, of the energy deposition distribution, $I = M_1^2/M_2M_0$

Swank RK, Absorption and Noise in X-ray Phosphors, J. Appl. Phys., 1973

d - SNR and DQE for a SPECTRUM of Xray Energies.

Signal and Noise for a a spectrum of xray energies	NEQ (i.e. SNR²) and DQE for a a spectrum of xray energies
$S = \int_0^{kV} \eta_S(E) E \Phi(E) dE$	$Q_{ideal} = \frac{\left[\int_0^{kV} E\Phi(E) dE\right]^2}{\int_0^{kV} E^2 \Phi(E) dE}$
$\sigma_s^2 = \int_0^{kV} \eta_{\sigma_s}^2(E) E^2 \Phi(E) dE$	$DQE(0) = \frac{S^2/\sigma_s^2}{Q_{ideal}}$

Separate integral for signal and noise are required for a spectrum of energies.
This was not made clear in Swank 73.

with S and σ_S determined from the integrals on the left.

e – Signal difference and relative contrast

In lecture L05, we saw that a small object which perturbs the attenuation of the surrounding material results has a relative contrast given by the difference between the attenuation coefficient of the small detail (i.e. the target material) and the attenuation coefficient of the surrounding material (i.e. the background material).

$$C_r = (\mu_t - \mu_b)\delta_t$$

From Lecture 05

When considering poly-energetic beams, the energy dependent transmission and detector signal efficiency must be accounted for when determining C_r. In the derivation, there is a transmission term of the form $exp(-\mu(E)\delta_t)$ that occurs within the integrations over pathlength and energy that lead to the signal in the target region, S_t, and the signal in the background region, S_b. For a small target, the attenuation difference comes from the difference in $\mu(E)$ over the region of the target, $\mu_t(E) - \mu_b(E)$. When $[\mu_t(E) - \mu_b(E)]\delta_t$ is small, these equation yield;

$$C_r = \frac{\int \eta_s(E) E \phi(E) [\mu_t(E) - \mu_b(E)] \delta_t dE}{\int \eta_s(E) E \phi(E) dE}$$

e – Signal difference and relative contrast

If we define the effective attenuation as a weighted average of $\mu(E)$,

$$\mu^{eff} = \frac{\int \eta_s(E) E \phi(E) \mu(E) dE}{\int \eta_s(E) E \phi(E) dE}$$

then C_r can be expressed as,

$$C_r = (\mu_t^{eff} - \mu_b^{eff})\delta_t$$

The effective attenuation coefficient, μ_{eff}, is defined with respect to:

- An x-ray spectrum incident on a target, $\phi(E)$.
- A detector with energy dependent absorption, $\eta_s(E)$.

Note: Some textbooks may define an effective attenuation coefficient that applies to other problems. For example, the transmitted exposure may be considered rather than a detector signal.

VI.C.5 – Rapid Sequence Acquisitions & fluoroscopy (15 charts)

5) Rapid Sequence Acquisitions & fluoroscopy
   a. Traditional fluoroscopy with Image Intensifiers.
   b. Pulsed Digital fluoroscopy
   c. Digital Angiography

VI.C.5.a – Historical fluoroscopy

From Lecture 01

- As was noted in L01, real time viewing of x-ray images (fluoroscopy) dates back almost to the discovery of the x-ray.
- Excessive radiation dose was encountered in Edison's early work on fluorscopy.
- To reduce dose, fluoroscopy was done in dark rooms after the radiography had become dark adapted (10-15 minutes).
- This continued until about 1950 when image amplification devices became available.

1933 photograph taken at the Mayo Clinic

VI.C.5.a – X-ray Image Amplification

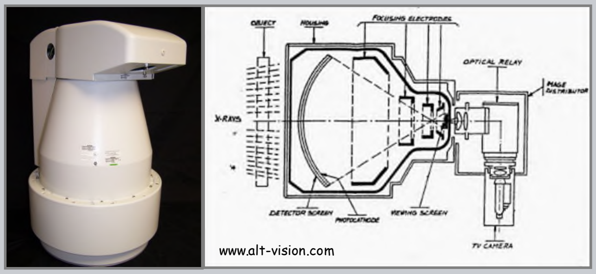

- X-ray Image Intensifies use CsI scintillations to detect x-ray and a photocathode to convert the light into electrons.
- Electrons are accelerated towards an output phosphor using high voltage, ~30 kV. The electron path is controlled by focusing electrons such that the image on the output phosphor is a mirror image of the input.
- Amplification is achieve by both minification and electron kinetic energy.
- The output phosphor image is then recorded with a TV camera or cine film.

VI.C.5.a – X-ray Image Amplification

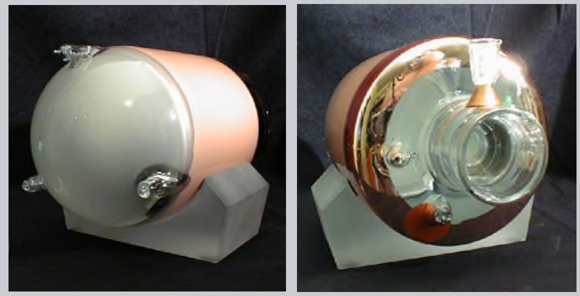

Front and back view of the glass vacuum tube of a Philips x-ray image intensifier.

VI.C.5.a – Rapid Sequence Angiography

Articulated C-arm devices provide flexible positioning for angiographic studies.

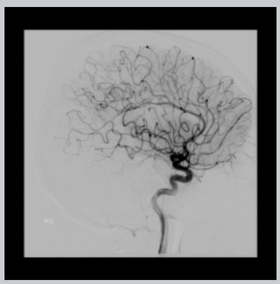

Pulsed image acquisitions at 2 to 4 frames per second depict the flow of iodinated contrast injected in veins or arteries.

VI.C.5.b – Pulsed Digital Fluoroscopy

Modern system now use solid state x-ray image detectors for pulsed fluoroscopic and rapid sequence acquisitions. The detector assembly is more compact that the image intensifier systems previously used.

From Cowen 2008

VI.C.5.b – Digital Fluoroscopy

CsI scintillators with TFT photodiode arrays are supplemented with flash lamp assemblies to rapidly erase the residual charge that would othewise create lag in the image response.

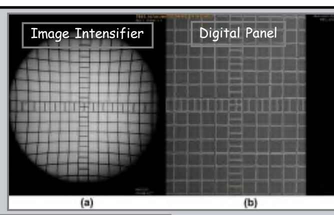

The photodiode array geometry produces images with no distortion.

The electron optics of I.I. systems results in distortion influenced by magnetic fields.

From Cowen 2008

VI.C.5.b – Pulsed Digital Fluoroscopy

Image Intensifier TV systems, IITV, can have reduced DQE at high exposure due to instrument noise in the readout cameras..

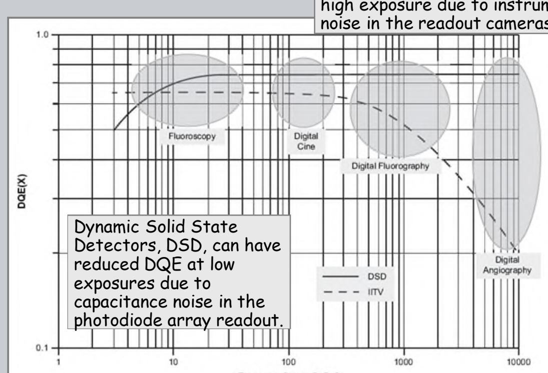

Dynamic Solid State Detectors, DSD, can have reduced DQE at low exposures due to capacitance noise in the photodiode array readout.

From Cowen 2008

VI.C.5.b – Pulsed Digital Fluoroscopy

Fluoroscopy with continuous radiation results in blurred images with blur. Fluoroscopy with short pulses of radiation reduces blur for the individual frames of the exam. Recorded cine images can be stopped with and show good detail.

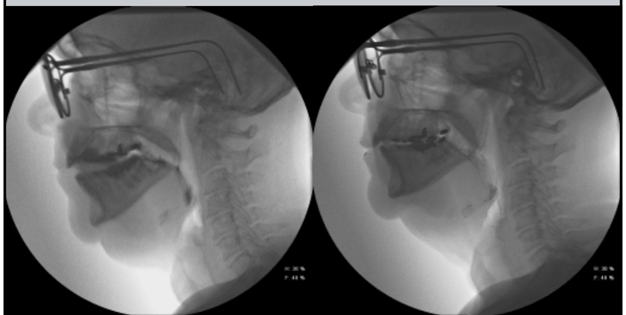

Continuous Fluoro   Pulsed Fluoro

Images From P. Rauch

VI.C.5.b – Pulsed Digital Fluoroscopy

Images From P. Rauch

These cine clips illustrate the difference between continuous and pulsed fluoroscopy using a toy car traveling on a circular track.

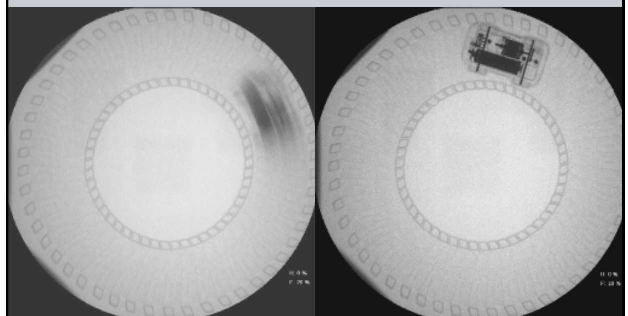

Continuous Fluoro   Pulsed Fluoro

VI.C.5.b – Pulsed Digital Fluoroscopy

A radiograph of a clock mechanism details the gears with low quantum noise.

Images From P. Rauch

VI.C.5.b – Pulsed Digital Fluoroscopy

Individual fluoroscopic frames have higher noise due to the low exposure per frame. These examples have the same exposure/frame but different frame rates.

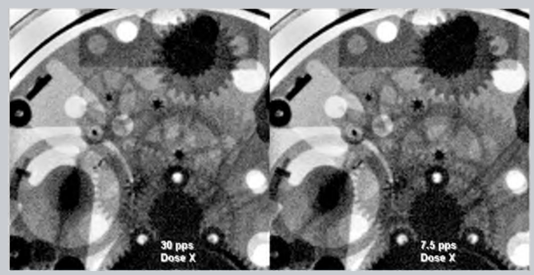

When shown as a movie clip, the higher frame rate has less noise because of temporal averaging by the human visual system.

Wilson DR, Perception of Temporally Filtered X-ray Fluoroscopy Images, Med. Phys. v21, pp245-256, 1994

Images From P. Rauch

VI.C.5.c –Digital Angiography

- Vascular disorders such as aneurisms and occlusions can be diagnosed using a rapid sequence of images obtained during the injection of iodinated contrast material.
- The sequence at the left demonstrates the flow of the contrast material through the right and left femoral arteries.

- On the right, the first frame has been subtracted from all frames

VI.C.5.c –Digital Angiography

Cerebral Angiogram

Arterial Phase

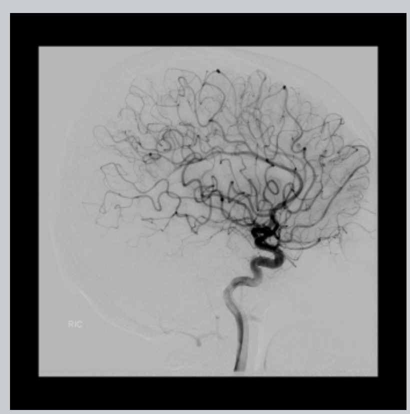

VI.C.5.c –Digital Angiography

Cerebral Angiogram

Perfusion Phase

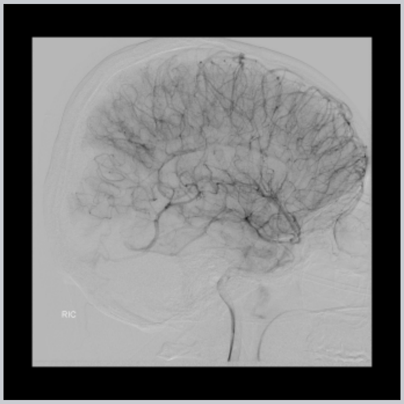

VI.C.5.c –Digital Angiography

Cerebral Angiogram

Venous Phase

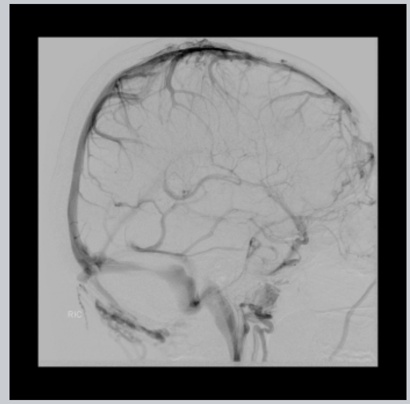

VI.C.6 – Active Pixel Detectors (3 charts)

6) Active Pixel Detectors
   a. Active Pixel circuits
   b. CMOS device performance

VI.C.6 – Active Pixel Detectors

The amorphous Si panels described earlier for digital radiography detectors have Passive Pixels Sensors (PPS). That is, the charge signal is stored on a capacitor and communicated through the readout line to the ADC with no active amplification.

The long length of the read-out lines limits performance.

- High capacitance results in high electronic noise (~2000 e's)
- Trapped charged leads to significant lag from frame to frame.

Active Pixel Sensors (APS) overcome the drawbacks of conventional detectors by using a pixel amplifier that improve SNR.

- Small pixel areas with smaller signals.
- Rapid sequence acquisitions with minimal lag.

VI.C.6 – CMOS Active Pixel Detectors

a-Si PPS equivalent circuit

A single thin film transistor (TFT) is used as a switch to allow charge to be read by an external preamp/ADC. Cdata is the capacitance associated with the column readout lines.

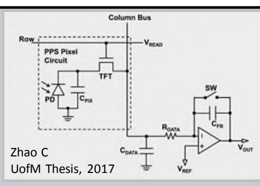

Zhao C
UofM Thesis, 2017

CMOS APS equivalent circuit

A typical 3 transistor CMOS panel readout circuit.

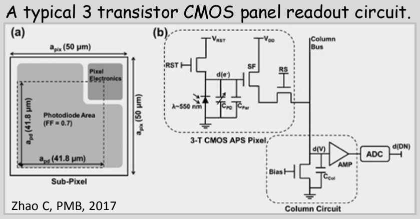

Zhao C, PMB, 2017

Transistors
RST: reset
SF: source follower
RS: row select

Capacitors
Cpd: photodiode
Cpar: parasistic
Ccol: column line

VI.C.6 – CMOS detector performance

Teledyne DALSA Professional Imaging

	High Sensitivity	H. Dynamic Range
Pixel Size, um	99	99
Readout Noise (e-)	140	340
Conversion (e-/xray)	490	490
NED, nGy	3.2	21.0

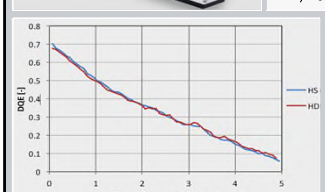

Maes WH, Peters IM; Low-dose performance of wafer-scale CMOS-based X-ray detectors, SPIE Medical Imaging, 2015.

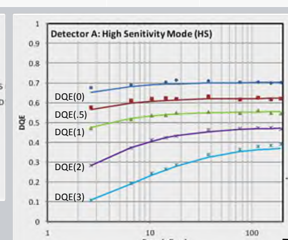

VI.C.7 – Photon Counting Detectors (6 charts)

7) Photon Counting Detectors
   a. CdTe detectors
   b. Si strip detector
   c. Energy weighted signals

VI.C.7.a CdTe detectors

PiXirad

Photon-counting, direct conversion, x-ray sensor.
- CdTe X-ray sensor, 0.65 mm thick
- 30 mm x 25 mm per module (1 to 8 modules).
- 60 micron hexagonal pitch
- Energy thresholds for each pixel
- CMOS ASIC

http://www.pixirad.com/

The PiXirad technology was developed at INFN, Italy (i.e. the Italian National Institute for Nuclear Physics).

VI.C.7.a CdTe detectors

- The CdTe sensor (Acrorad Co. Ltd, Japan) is a Schottky diode with electron collection.
- Very low leakage current @400-500V bias.
- Hexagonal array charge readous

CdTe semiconductor characteristics	
Atomic numbers	48, 52
Effective atomic number	50
Density ρ(g/cm³)	5.85
Band energy (eV)	1.5
Dielectric constant	11
Ionizing energy (eV)	4.43
Resistivity ρ(Ωcm)	10^9
Electron mobility μ_e (cm²/Vs)	1100
Electrons mean lifetime τ_e (s)	$3x10^{-6}$
Hole mobility μ_h (cm²/Vs)	100
Holes mean lifetime τ_h (s)	$2x10^{-6}$
$(\mu\tau)_e$ (cm²/V)	$3.3x10^{-3}$
$(\mu\tau)_h$ (cm²/V)	$2x10^{-4}$

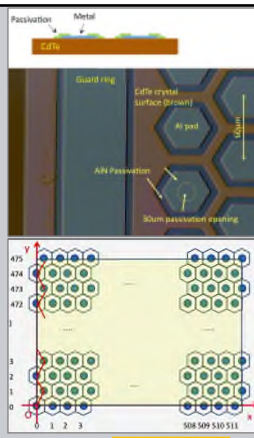

The reported material properties are consistent with those in Lecture 08.

PiXirad

VI.C.7.a CdTe detectors

PiXirad

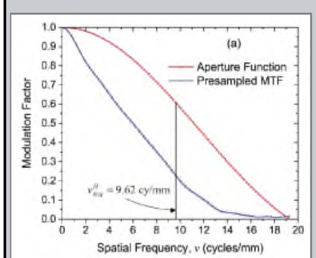

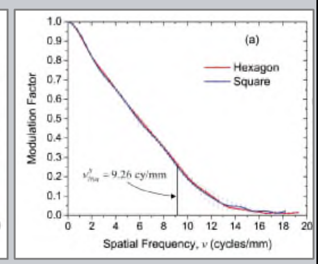

- Charge sharing causes the MTF to be significantly reduced from the aperture function MTF associated with ideal charge collection.

Vedantham, Med. Phys., May 2016.

- Row and column pixels are interpolated from the three hexagonal signals surround each pixel in a square array.
- The interpolation has minimal effect on the MTF.

VI.C.7.a CdTe detectors

- The energy resolution measure from a cluster of 1000 pixels demonstrated a dependence on enery consistent with the statistical charge variation.
- The equivalent noise charge of the ASIC is 50 electrons.

Energy [keV]	FWHM [keV]	Resolution %
2.96	0.76	25.8
4.95	0.85	17.1
8.1	0.88	10.8
10	0.92	9.2
12	1.06	8.8
14	1.20	8.6
16	1.31	8.2
18	1.48	8.2
22	1.38	6.3
38	1.60	4.2
59.54	1.73	2.9

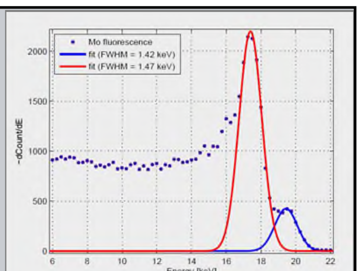

(b) Molybdenum fluorescence lines K_α and K_β.

Over half of the counts are from charge sharing (6-15 keV) which can produce multiple counts in different pixels from one incident x-ray. This results from either radiation transport or charge diffusion.

Vincenzi, J. Inst., April 2015.

PiXirad

VI.C.7.a CdTe detectors

XCounter

Dual Energy photon-counting, direct conversion, x-ray sensor for digital x-ray imaging.
- CdTe – CMOS detector (12 bits)
- 0.75 mm – 2.00 mm CdTe thickness
- 100 micron detector elements
- 1536 x 128 detector array
- Up to 1000 fps

https://xcounter.com/

VI.C.7.a CdTe detectors

XCounter

Anti Charge Sharing (ACS)

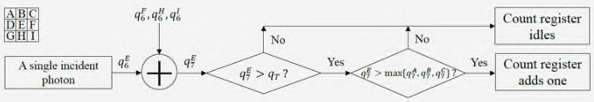

The Xcounter CdTe detector processes the signal from each detector element to improve image quality. Anti Charge Sharing (ACS) compares the charge from each pixel to that of it's neighbors to prevent multiple counts due to fluorescent radiation emitted from Cd or Te atoms (see above).

An energy threshold is used to accept only charge depositions above the designated threshold.

Both ACS and energy threshold processing prevents correlated noise and produces a flat noise power spectrum (NPS).

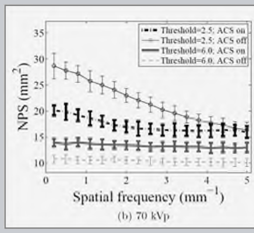

Ji X, SPIE Medical Imaging, vol. 10132, Mar. 2017.

VI.C.7.b Si strip detector

Philips MicroDose Mammography System

- Si Strip Detector
- 50 micron pixels
- Tungsten anode, 0.5mm Al filter
- Energy weighted signal
  - High energy depositions
  - Low energy depositions

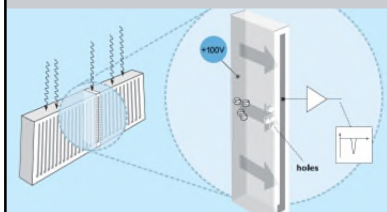

Note: Philips purchased MicroDose from Sectra in 2011

VI.C.7.b Si strip detector

Aslund et. al., Medical Physics, 2007

Physical characterization of a scanning photon counting digital mammography system based on Si-strip detectors

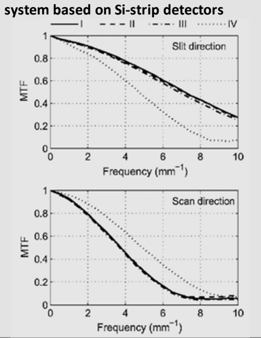

The noise power spectrum (NPS) for the Si strip detector is reported by normalization to the ideal NPS (see Lecture 7).

N(w) = NPS(w) x Qi

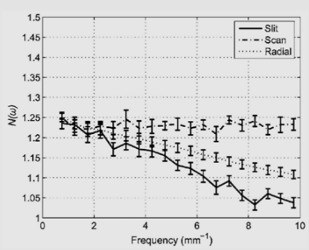

Fig. 4. Average of 12 measures over an input exposure range from 21 to 2006 microGray.

VI.C.7.b Si strip detector

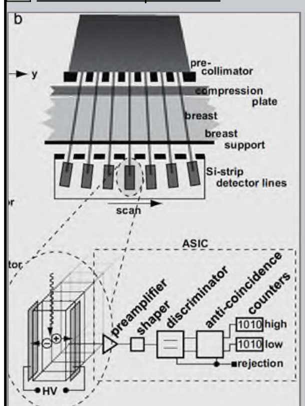

Fredenberg et. al., NIM A, 2010

Energy resolution of a photon-counting silicon strip detector

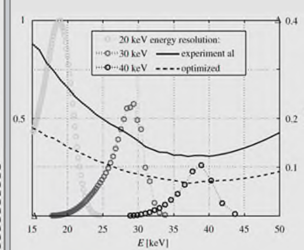

Fig. 7. Energy response on monochromatic delta peaks.The plotted peaks are for the experimental detector. Energy resolution (dE/E) is shown for the experimental detector, and for an improved detector with high AC efficiency and low threshold spread and electronic noise.

VI.C.7.b Si strip detector

Berglund et. al., SPIE MI, 2014

Energy weighting improves the image quality of spectral mammograms: Implementation on a photon-counting mammography system.

"We have implemented and evaluated so-called energy weighting on a commercially available spectral photon-counting mammography system. A practical formula for calculating the optimal weight from pixel values was derived. Computer simulations and phantom measurements revealed that the contrast-tonoise ratio was improved by 3%–5%, and automatic image analysis showed that the improvement was detectable in a set of screening mammograms."

The simulated CNR improvement is shown as a function of weight. The CNR improvement and optimal weight were larger for higher tube voltages. A weight of ~1.8 is near optimal for all cases.

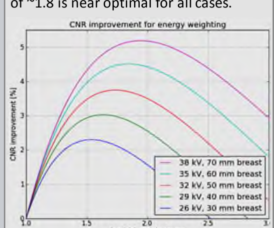

50 micron calcification in breast tissue.
18 keV threshold @ 26 kV
20 keV threshold @ 32 kV
22 keV threshold @38 kV

VI.C.7.c Energy Weighted Signals

Cahn et. al., Medical Physics, 1999

Detective quantum efficiency dependence on x-ray energy weighting in mammography.

"..transmitted low energy photons carry more contrast information than transmitted photons of higher energy. Energy-integrating detectors will put a weight factor to each photon proportional to its energy and the weighting will thus be contrary to the information content."

A generalized expression for the detector signal is a weighted sum of the discrete fluence spectrum.

$$S = \sum_{i=1}^{m} w_i \emptyset_{Ei}$$

- $w_i = 0$ is the case of a photon counting detector.
- $w_i = E$ is the case of an energy integrating detector

Using an approach similar to Tapiovaara1985, Cahn shows that a more optimal weight will optimize the contrast to noise, CNR, for a small target (t) in a uniform background (b).

For high Z targets, the weights will be proportional to E^{-3} due to photoelectric absorbtion.

$$w_i \propto \left(1 - e^{-\left(\mu_{Ei}^t - \mu_{Ei}^b\right)\delta_t}\right)$$

$$w_i \propto \left(\mu_{Ei}^t - \mu_{Ei}^b\right)\delta_t \text{ , small } \delta_t$$

From Lecture 05: $C_r = (\mu_t - \mu_b)\delta_t$

Cahn et. al. , Medical Physics, 1999

Detective quantum efficiency dependence on x-ray energy weighting in mammography.

TABLE II. DQE for different objects in a mammography image for a W spectrum in (a) and for a Mo spectrum in (b). The DQE is indicated for charge integration, photon counting and also assuming weight factors proportional to E^{-3}, the latter is close to the optimum in mammography.

	Integrating	Photon counting	Weight $\propto E^{-3}$
(a)			
100 μm microcalcification	0.74	0.84	1.00
250 μm microcalcification	0.77	0.87	0.99
500 μm microcalcification	0.81	0.90	0.98
2.5 mm tumor	0.71	0.82	1.00
5.0 mm tumor	0.72	0.83	1.00
10.0 mm tumor	0.74	0.85	1.00
(b)			
100 μm microcalcification	0.70	0.84	1.00
250 μm microcalcification	0.72	0.86	1.00
500 μm microcalcification	0.76	0.89	0.99
2.5 mm tumor	0.68	0.83	1.00
5.0 mm tumor	0.68	0.83	1.00
10.0 mm tumor	0.70	0.85	1.00